Engineering Failure Analysis 152 (2023) 107526

Contents lists available at ScienceDirect

Engineering Failure Analysis

journal homepage: www.elsevier.com/locate/engfailanal

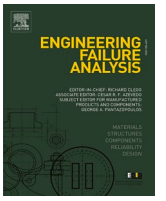

Development of an experimental/numerical validation methodology for the design of exhaust manifolds of high performance internal combustion engines

Mariano Lorenzini [a], Saverio Giulio Barbieri [b,*], Valerio Mangeruga [b], Matteo Giacopini [b]

[a] Ferrari SpA, Structural Calculation Division, via Abetone Inferiore 4, I-41053 Maranello (MO), Italy
[b] University of Modena and Reggio Emilia, Engineering Department Enzo Ferrari, via Vivarelli 10, 41125 Modena (MO), Italy

ARTICLE INFO

Keywords:
Exhaust manifold
Finite elements method
Thermal fatigue
Plasticity

ABSTRACT

Several typical failure modes in the exhaust manifold of an internal combustion engine are commented on. In particular, thermal loading and the related thermal fatigue damage mechanism are addressed. The component under investigation is a cast exhaust manifold including the turbine involute. Finite Element simulations are performed, and a numerical methodology is presented to interpret and understand the observed failures, with the aim of developing a useful tool to virtually validate the component, before the manufacturing phase. The Finite Element analysis closely mimics the experimental validation procedure that considers several heating and rapid cooling cycles to simulate typical engine operating conditions. A static mechanical characterization at high temperatures of the materials involved is carried out, aimed at identifying a suitable alloy and its mechanical characteristics useful for feeding the numerical models. The developed design methodology proposes a damage criterion for thermal fatigue investigation, considering the elastoplastic behaviour of the material when subjected to high temperature cycles. In particular, the accumulated equivalent plastic strain range for a single thermal cycle (ΔPEEQ) is used, following the Ferrari expertise. The methodology appears to be well correlated with the experimental evidence, thus limiting the number of tests necessary for the approval of the component.

1. Introduction

Compliance with stringent engine emissions standards and pressing demands for higher performance strongly drive the design of modern internal combustion engines to increase their efficiency. Turbocharging (downsizing), high compression ratios, advanced spark-ignition strategies are some of the solutions adopted. As a result, the engine components are subjected to higher specific loads leading to higher mechanical and thermal loads [1–4]. Therefore, the design procedures for structural and thermo-structural analyses of engine components have to be constantly improved [5,6]. Alternative materials and both innovative design methodologies and manufacturing techniques [7–9] are usually employed with the aim of minimizing the mass of engine components, while ensuring

* Corresponding author.
E-mail addresses: mariano.lorenzini@ferrari.com (M. Lorenzini), saveriogiulio.barbieri@unimore.it (S.G. Barbieri), valerio.mangeruga@unimore.it (V. Mangeruga), matteo.giacopini@unimore.it (M. Giacopini).

https://doi.org/10.1016/j.engfailanal.2023.107526
Received 18 June 2023; Received in revised form 21 July 2023; Accepted 1 August 2023
Available online 2 August 2023

Nomenclature

BSD	backscatter electron detector
E	elastic modulus
EDX	energy dispersive x-ray
EF	elongation at fracture
FE	Finite Elements
K'	first characteristic parameter of the material
N_f	number of cycles to failure
R_p02	yield strength
SEM	scanning electron microscope
UTS	ultimate strength
ΔPEEQ	the equivalent plastic strain range registered for a single thermal cycle
ΔWp	plastic work
α	thermal expansion coefficient
α'	second characteristic parameter of the material
ε_{ap}	alternating plastic strain
ε_e	elastic strain
ε_p	plastic strain
$\bar{\varepsilon}^{pl}\big\vert_0$	equivalent initial plastic strain
$\dot{\bar{\varepsilon}}^{pl}$	equivalent plastic strain rate
ε_t	total strain
λ	thermal conductivity
σ	stress
σ_a	alternating stress
σ_y	yield strength

continued durability and reliability.

Exhaust manifolds are fundamental components in internal combustion engines, and they usually have complex geometries, the result of a compromise between minimum weight, adequate dimensions and maximum thermodynamic performance. Thermal loads play a crucial role in the structural validation of these components. Indeed, the related low cycle fatigue phenomena are well known to be the most common cause of exhaust manifold failure [10–14]. In 2014, Yan et al. [15] applied a coupled CFD – FEM methodology to predict structural failure of exhaust manifolds and they found that the first natural frequency led to high cycle fatigue collapse. In this case, however, a naturally aspirated engine was considered, and the plastic strains were not predominant. In the same year, Chen et al. [16] studied the thermomechanical behaviour of an exhaust manifold for a turbocharged gasoline engine and proposed a methodology to simulate the structural failure of the component due to plastic deformations. Charkaluk et al. [11,17,18] proposed a computational methodology to quantify thermomechanical fatigue damage using an energetic approach. The present work resumes these last researches and adopts a simplified approach, more suitable for a typical industrial design flow, especially during the early stages of the component development process. In particular, ΔPEEQ (the equivalent plastic strain range registered for a single thermal cycle) is the key parameter of plastic deformation and it has been correlated to the number of thermal cycles to failure.

In the literature, the usage of the equivalent total strain range is also adopted as a reference parameter to quantify the material's stress [19,20]. In this contribution, only the plastic part is considered, since in this particular application plastic strain is dominant with respect to the elastic counterpart.

The paper is organized as follows. First of all, the validation tests used by Ferrari in the typical component development process are described, and the most common anomalies found on the initial geometry configurations of the exhaust manifold are shown. In particular, two different exhaust manifold geometries named Engine C and Engine B configurations are analysed. Then, a static high-temperature characterization of the materials involved is presented and an alloy with suitable mechanical properties is proposed. The effects of the thermal load are studied through Finite Element simulations that mimic Ferrari validation tests. A modelling strategy aimed at reproducing the time history of the temperature profile of the exhaust manifold is therefore presented and the relative stress and strain distributions characterizing the typical use of this component are then shown. A low-cycle thermal fatigue criterion based on the equivalent plastic strain range registered for a single thermal cycle (ΔPEEQ) is described and the corresponding results are shown and compared with the experimental evidence. Finally, some conclusions end the paper.

2. Material and methods

2.1. Validation cycle tests

The typical experimental investigation flow for internal combustion engines includes a fairly large number of tests for the

validation of all the components. According to Ferrari standards, several tests are usually required to check the reliability of the exhaust manifolds, two of which are specifically related to thermal fatigue verification: *Engine Life* test and exhaust manifold *Thermal Shock* test. The former is a complete test of the engine assembly where all the components must maintain their structural integrity in order not to compromise the functionality of the unit. The second is a specific test for the exhaust manifolds and evaluates the possible failures related to sudden changes in temperature that could affect the component during its life.

2.1.1. Engine Life cycle

The experimental tests of durability, called *Engine Life* cycle, are performed for the functional and reliability validation of the entire engine during the actual use of the vehicle. The test consists of a succession of stationary times with low and high engine loads. The engine assembly is fully representative of the actual installation, all test bench-vents are switched on, and the operating and surrounding conditions mimic a typical engine application. From the thermal point of view, the temperature varies cyclically 7500 times between a minimum and a maximum value. The test cycle mainly consists of ramps at full engine load, followed by a stationary phase under conditions of maximum power at rated speed. After each cycle, a rest interval at idle speed is introduced which allows the components to cool down. The test is successfully passed if the engine maintains acceptable performance levels without any serious component reliability shortcomings until the end of the experiment. This is undoubtedly a conservative specification for most of the components involved, but at the same time, it must be emphasized that the thermal loads do not reach the high levels that could occur during the vehicle operation. In particular, the temperature range is limited since the engine off condition is never encountered during the test.

2.1.2. Thermal Shock cycle

The so-called *Thermal Shock* cycle is a specific engine bench test for the validation of exhaust manifolds only. The *Thermal Shock* cycle consists of a cycle of extreme temperature at the limit of engine capabilities, i.e. a sequence of rapid heating and cooling cycles that attempt to reproduce typical damage due to thermal fatigue phenomena. For this test, all parts that can influence the temperature distribution of the exhaust manifold are used, such for example the heat shields that can act as a thermal barrier to irradiation phenomena and affect the convection heat transfer of the air flowing through the outside the manifold. In the heating phases, a specific calibration of the combustion process is employed to increase the heating gradient and thus reach a condition of maximum stationary temperature on the external surface of the manifolds in the shortest possible time. For this purpose, the ventilation of the test room for cooling the manifolds and the turbocharger is also deactivated. During the cooling phase, the throttles are opened and the engine, powered off, is motored to blow fresh air into the manifold. The test bench ventilation systems are activated to speed up the cooling of the external surfaces. This thermal cycle does not reflect actual vehicle usage, it represents an extreme loading condition in terms of maximum temperature range and rate of heating and cooling. This test is successfully passed if, after 1000 cycles, no through cracks are detected and consequent gas leakage on the exhaust manifolds. Furthermore, cracks with loss of material from the internal surfaces of the manifold are not tolerated, because they could promote damage of the impeller of the downstream turbine.

2.1.3. Experimental measurements of the temperature cycles

The temperature profile during the *Engine Life* and *Thermal Shock* cycles is usually measured to characterize the test conditions of the exhaust manifolds. These data are then commonly employed for the calibration of the Finite Element models. For the sake of brevity, only the results related to one of the tested configurations are presented in the following. In this specific case, thirty-six surface thermocouples have been installed, eighteen each manifold, and temperatures have been measured during the tests. Fig. 1 shows the detail of the set-up of the surface thermocouples on the left-side manifold. The configuration and the results of the right-side manifold are mirrored, and they are omitted in the following.

Thermocouples have been distributed to cover the characteristic areas of the geometry. Points 1-2-3-4 have been positioned in the

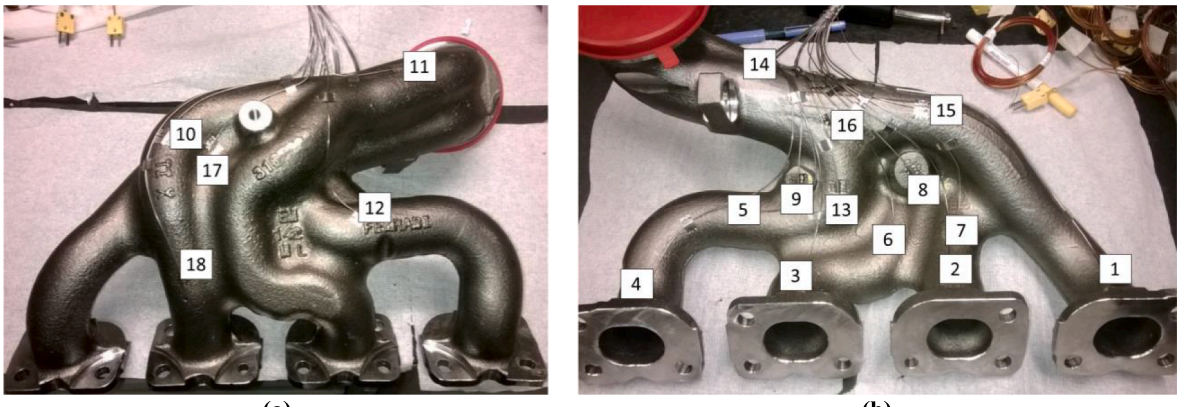

Fig. 1. Experimental temperature measurements using surface thermocouples;(a) front view; (b) rear view.

initial part of the manifold where the primary ducts are still separated from each other and where the thermal state can be influenced by conduction heat transfer with the engine head. The thermocouples 5-6-7-8-9-13-15-16 have been positioned in the internal central area facing the engine, which is the massive part of the manifold. In particular, points 8 and 9 identify the casting points, required by the casting process of the component. Points 10-12-17-18 have been selected on the outer side of the manifold to compare the possible temperature differences with respect to the internal surfaces facing the engine. The external areas of the manifold are more accessible and are certainly subjected to a greater flow of air promoted by the forced ventilation of the test bench. Finally, points 11 and 14 have been placed at the end of the manifold on the secondary ducts.

Fig. 2 shows the temperature versus time profile for the *Engine Life* cycle, while Fig. 3 depicts the results of the *Thermal Shock* cycle. It is worth noting that each cycle of the *Engine Life* approximately lasts twice as long as the *Thermal Shock* cycle. However, the specific time scale has not been reported due to reasons of company confidentiality. The *Thermal Shock* cycle represents an extreme thermal transient condition. In less than a minute, a maximum temperature of almost 900 °C is reached and the difference between the maximum and minimum temperature is approximately 750 °C. In the *Engine Life* cycle, the maximum stationary temperature is comparable to that reached during the *Thermal Shock*, but less severe thermal gradients and oscillations are encountered.

The *Thermal Shock* cycle is significantly different from standard usage conditions, but it is useful for the calibration of numerical models. On the contrary, the *Engine Life* cycle mimics the maximum power state and, therefore, provides information about the actual thermal field and how it is affected by the applied boundary conditions.

2.2. Experimental evidence

In the following, several structural anomalies found during these experiments are collected.

The tested components have been studied considering different levels of accuracy and both non-destructive and destructive investigation techniques have been employed. First, a visual analysis of the component still assembled in the test room has been performed to identify the so-called blocking ruptures, i.e. failures that compromise the functionality of the component and that force the test to be halted. The soap bubble test is the most commonly used procedure: the component is prayed with a soap and water solution and compressed air is blown into the manifold. Any through crack of the component is easily detectable by the formation of localized foam and bubbles. This test can be performed with a fully assembled engine, so its impact on the test timing is limited. On the other hand, only failures caused by through cracks can be detected. Dye penetrant testing is another common non-destructive visual analysis employed. However, this second experimental technique requires disassembly of the manifold.

It is also important to consider that the ruptures are rarely identified early. Indeed, in order to minimize the impact of crack detection and investigation on test time and cost, the number of checks prescribed along the test duration is limited. Therefore, any failures are detected only when the test is interrupted by a major functional loss of the component, or when the test is normally suspended by scheduled checks. With reference to the specific case of the manifold, when a failure is detected, a relative number of cycles to failure is assigned corresponding to the last successfully passed soap bubble test.

Going into the specific cases investigated, two V8 turbo engines have been analysed and compared, hereinafter referred to as C1 and B1; the manifold geometries of the two engines are completely different, but the operating conditions are similar.

The experimental results are discussed in the following. The C1 engine exhaust manifold failed during both the *Engine Life* and *Thermal Shock* cycles, while the B1 configuration failed only during the *Thermal Shock* cycle.

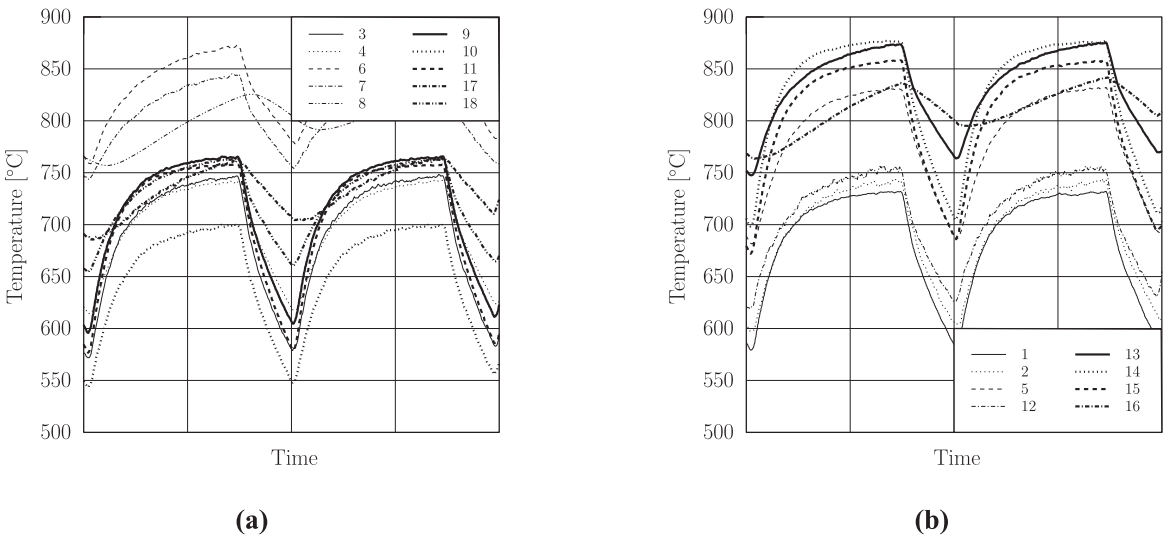

Fig. 2. Temperature profiles registered during the *Engine Life* cycle.

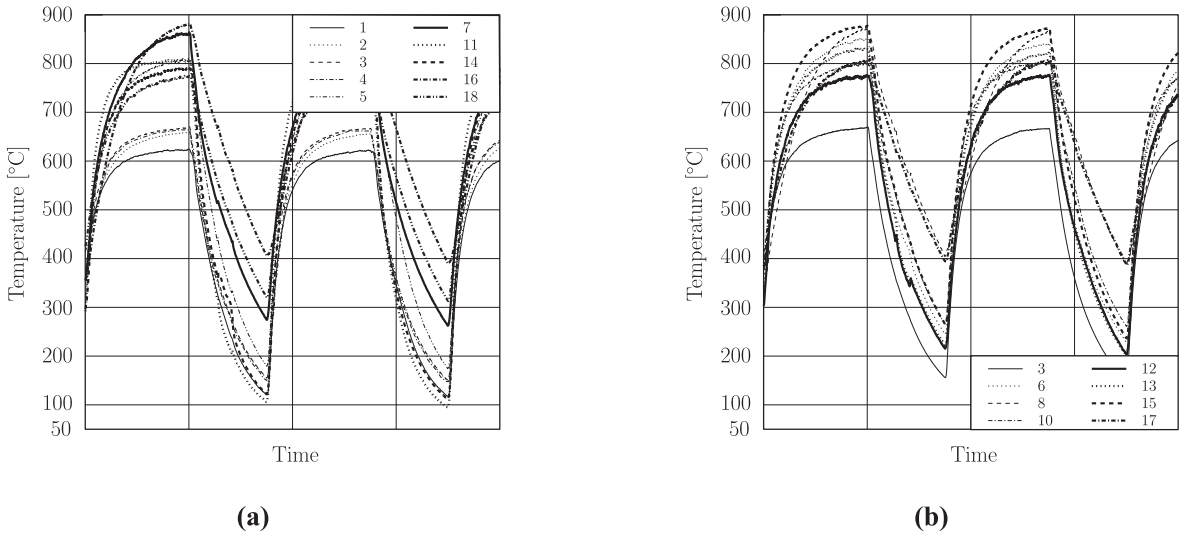

Fig. 3. Temperature profiles registered during the *Thermal Shock* cycle.

2.2.1. Experimental evidence of engine C1

First, the engine C1 has been tested and the *Engine Life* cycle has been applied. Five tests have been performed and failures have been detected during each experiment. The component underwent a minimum of 6300 thermal cycles before cracking appeared.

A first-level analysis has been performed using the soap bubble test. A pressure of 0.5 bar has been applied to the assembled manifold and a probable through crack has been detected at cylinder duct number 4, see Fig. 4. Therefore, the test has been stopped and the manifolds have been disassembled for further analyses.

Both the right and left manifolds have been examined in depth and through cracks have been found with fatigue propagation from the internal surface of the duct to the outside. There are also superficial cracks extending inward, not passing through but affecting a substantial part of the thickness. These failures have been repeatedly identified on all engines with equivalent manifold geometry.

Several laboratory tests have been then performed. Fig. 5 depicts the right and left exhaust manifolds and the areas showing fatigue cracks are highlighted by penetrating liquids. Crack 2, 3 and 4 in Fig. 5 (left manifold) are through ones, also identified by the soap bubble test.

Stereo microscope analyses of fracture surfaces have been accomplished after forcing cracks fully open. Fig. 6 refers to the left manifold and shows crack number 2, which exhibits arc propagation, see the white line, and presents concentric lines. This is a fatigue crack with a surface extent of approximately 7.5 mm and a propagation depth from the outer surface into the pipe interior of up to 3 mm. Casting defects at the nucleation point, indicated by the white arrow, are excluded.

Fig. 7 shows the results of the SEM (Scanning Electron Microscope) analyses of fracture number 2. BSD (Backscatter Electron Detector) has been employed to obtain Fig. 11(a), where a different colouring of the propagation surface can be seen. A subsequent

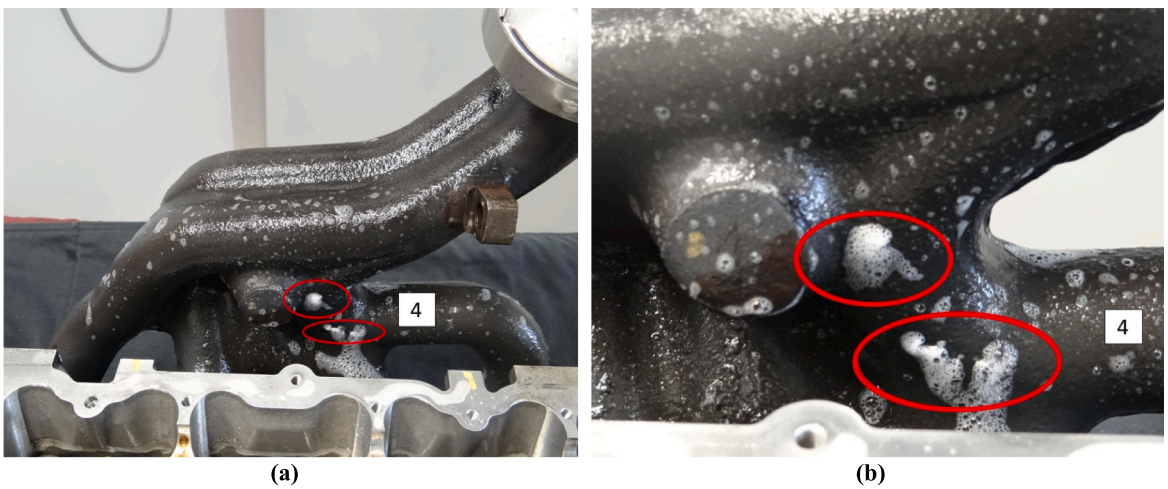

Fig. 4. Engine C1- Bubble test (a) the right-hand side exhaust manifold; (b) detail of the failure.

Fig. 5. Engine C1 – 1, 2, 3, 4 indicate failures identified by dye penetrant tests on the left-hand side exhaust manifold.

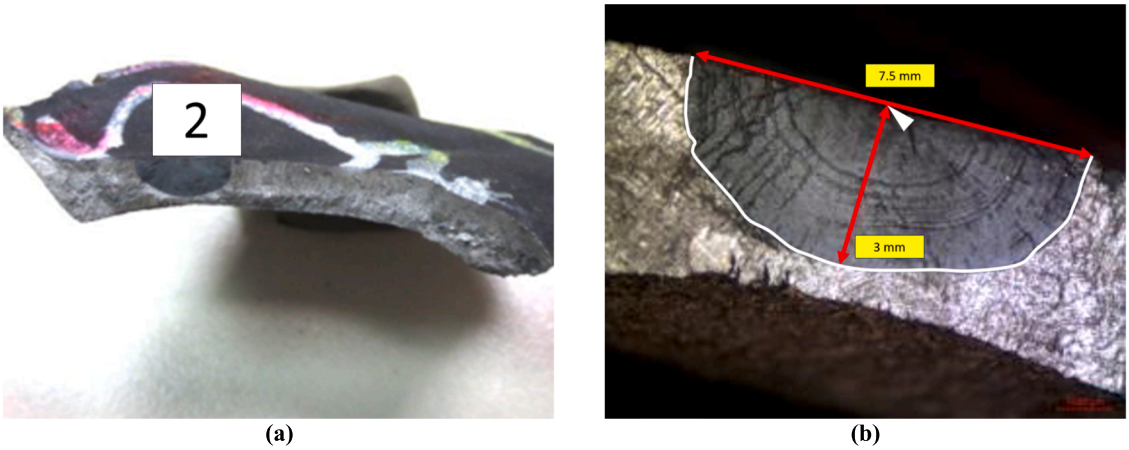

Fig. 6. Engine C1 - Crack 2 on the left-hand side exhaust manifold.

EDX (Energy Dispersive X-ray) analysis shows the oxidized surface, as a result of exposure to oxygen at high temperatures, see Fig. 11 (b). These figures show a common fatigue crack propagation possibly induced by thermal fatigue, characterized by an arc shape, see the white line, and the presence of concentric lines. The nucleation point is indicated by the white arrow.

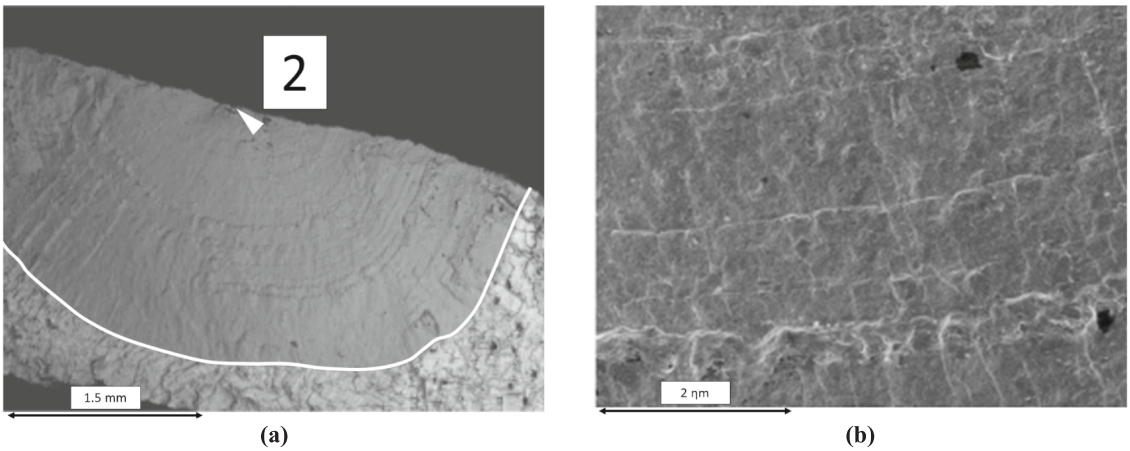

Fig. 7. Engine C1 - Crack 2 on the left-hand side exhaust manifold, SEM analyses.

The C1 engine has been also subjected to the *ThermalShock* cycle. Two tests have been performed and failures have been detected during both experiments. The minimum number of cycles performed without any rupture is 400.

In particular, both tests have been interrupted due to a serious leak of exhaust gases from the right manifold, which has caused a fire in the test room. The component has been disassembled and an almost total break has been found in the resistant section of duct number 4. Fig. 8 shows the results of the bubble test: a further through crack has been found on duct number 3 of the right manifold and two further through cracks on duct number 5 of the left manifold. The affected areas are very similar to the critical areas identified during the *Engine Life* test. The more severe *Thermal Shock* cycle has significantly accelerated crack nucleation and propagation. Given the size of the cracks and the similarities with those already analysed for the *Engine Life* cycle, no further analyses have been carried out.

2.2.2. Experimental evidence of engine B1

The B1 engine has been tested considering only the *Thermal Shock* cycle. Three tests have been performed and only one of the three was prematurely terminated by a macroscopic failure. The minimum number of cycles passed without any rupture is 500. Fig. 9 shows the results of the soap bubble test. Only one through crack has been found on the left manifold. Then, dye penetrant testing has revealed cracks in the same areas during all three tests on both the left and right manifold, Fig. 10. These results have been further investigated by laboratory analyses. The through crack detected on the left manifold has been opened completely. Fig. 11 shows a typical fatigue crack propagation from the exterior surface into the duct characterized by the typical arc shape, see the white line. The crack affects the entire thickness of the manifold and no casting defects have been found.

2.3. Material characterization

During the preliminary stages of the project, a static characterization of the materials at high temperatures (up to 1000 °C) has been performed in order to identify the most suitable alloy and obtain all the data necessary to feed the FE (Finite Elements) models. For the exhaust manifolds, two different stainless steel alloys for casting applications have been considered: a reference high temperature casting steel commonly adopted in similar applications where high mechanical strength and good corrosion resistance are required (hereinafter referred as Steel 1) and a custom casting steel (hereinafter Steel 2) specifically developed by adding niobium to the standard chemical composition to improve and maintain the mechanical characteristics at high temperatures [21].

For an in-depth discussion, fatigue tests should also have been carried out to have a complete comparison between the two materials and uniquely identify the most suitable one for this application. To avoid a long and time and cost consuming experimental campaign, it was decided to carry out a comparison based only on monotonic tensile tests in order to quantify the effect of the introduction of niobium on the mechanical strength of the material assuming then, on the basis of the literature, a corresponding increase in fatigue properties [22].

The Zwick Roell Z050 testing machine has been used for these static characterizations. Strain controlled tensile tests focused on high temperatures have been performed.

The monotonic σ-ε curve has been obtained at room temperature and in the temperature range between 400 °C and 1000 °C, chosen considering the data available in the literature [23] and considering that mechanical characteristics begin to substantially decay around 700 °C. As the number of specimens was limited, the tests have been concentrated around this temperature to have a greater density of experimental data in the interval where the most significant variations of the mechanical characteristics were expected.

A strain rate of 2 mm/min has been applied during the tests and all specimens have been conditioned at the specific test temperature for 48 h before completing the tensile test. A total of sixteen samples have been tested for each material.

In the specific case of exhaust manifolds, dissection specimens cannot be obtained directly from the components due to the complex geometry and limited thicknesses. Consequently, the characterization should be performed on specimens that reflect as closely as

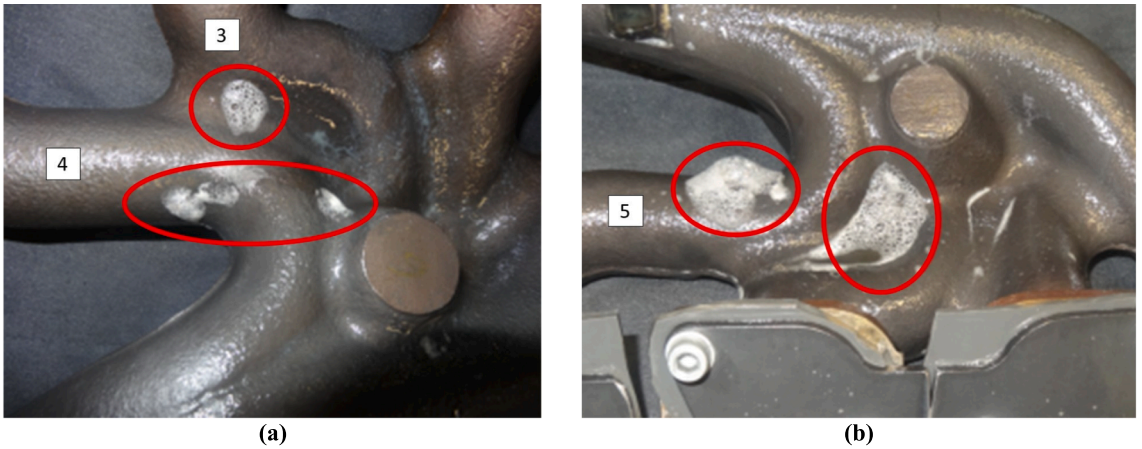

Fig. 8. Engine C1 - bubble soap test results, (a) right-hand side exhaust manifold, (b) left-hand side exhaust manifold.

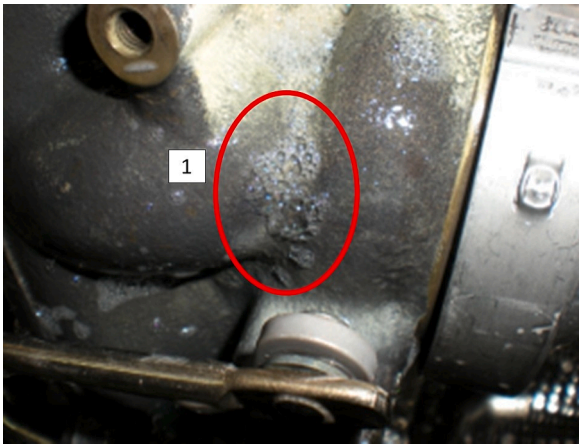

Fig. 9. Engine B1 – left-hand side exhaust manifold, soap bubble test results.

Fig. 10. Engine B1 – dye penetrant test results, (a) left-hand side exhaust manifold, (b), (c) right-hand side exhaust manifold.

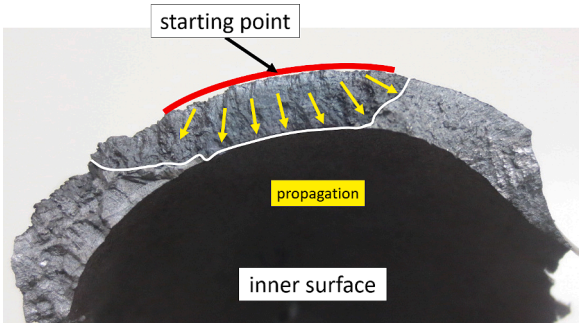

Fig. 11. Engine B1 – left-hand side exhaust manifold, detail of the through crack.

possible the actual characteristics of the final component. Therefore, the specific casting equipment and strategy used to manufacture the manifold have been employed to obtain the specimens. The gauge length of the specimens has been defined in order to correctly install the extensometer for the measurement of elongation and to obtain the most homogeneous temperature distribution possible.

Both the materials have been tested and the results have been collected in Figs. 12-15.

Figs. 12 and 13 show the main results obtained from the static characterization as a function of temperature of Steel 1 and 2 respectively; in particular E (elastic modulus), R_p02 (yield strength), UTS (ultimate strength), and EF (elongation at fracture) are reported.

Note that the properties of Steel 1 have been normalised against the values registered at room temperature while those of Steel 2 have been normalised against the corresponding values of Steel 1 for a direct comparison.

The tested materials showed similar properties. The experimental data exhibit evident trends, even if Steel 2 presents a dispersion in the range 600 °C – 700 °C in terms of ultimate strength. As the temperature increases, however, the results appear to be more repeatable. Experimental data confirm that ultimate strength begins to substantially decay around 700 °C.

For both materials, the difference between ultimate strength and yield strength appears to be minimal at temperatures above 800 °C. This behaviour can be easily explained by observing the full stress–strain curves in Figs. 14 and 15, which show that both

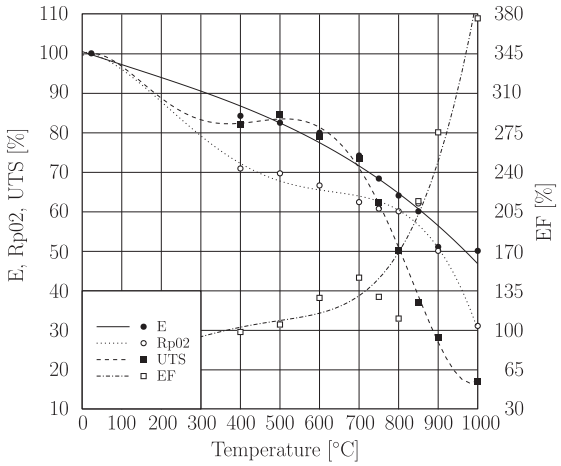

Fig. 12. Steel 1 (standard) - Static characterization as a function of temperature.

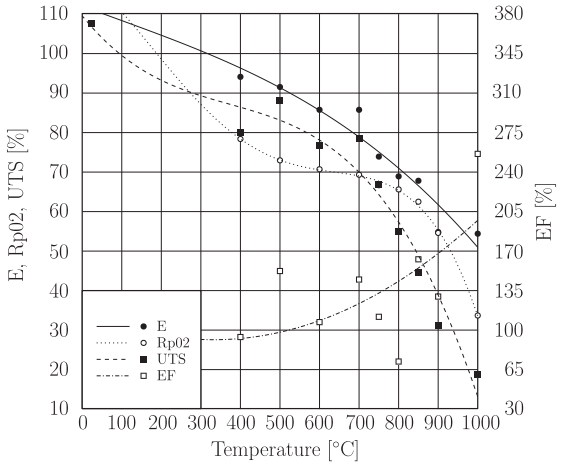

Fig. 13. Steel 2 (custom) - Static characterization as a function of temperature.

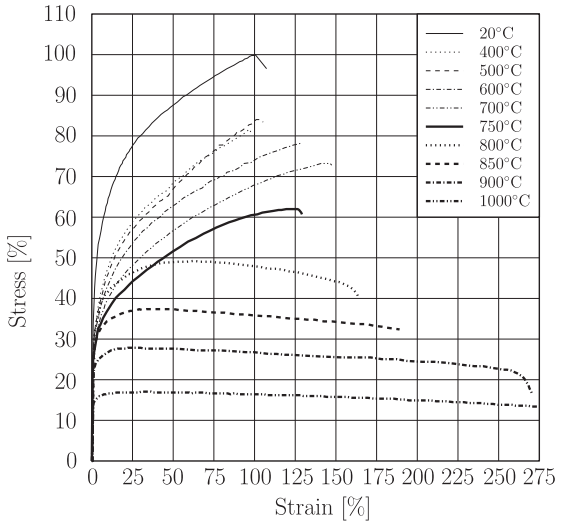

Fig. 14. Steel 1 (standard), stress–strain curves as a function of temperature.

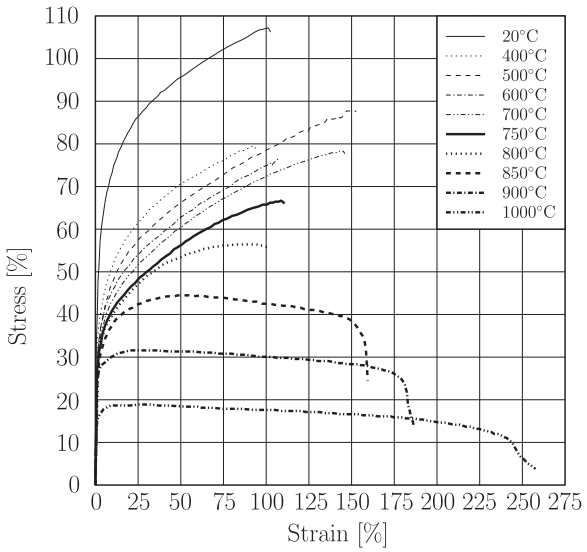

Fig. 15. Steel 2 (custom), stress–strain curves as a function of temperature.

materials essentially follow an elastic-perfectly plastic model. Note that results have been normalised with respect to the UTS and EF values of Steel 1 at room temperature.

Despite the minor differences, Steel 2 has been selected for the production of exhaust manifolds, as it exhibits (slightly) higher mechanical properties at maximum temperature (1000 °C).

3. Theory

3.1. Low-cycle fatigue

Generally, in the context of finite-life fatigue, a distinction is made between the low-cycle fatigue region, characterized by significant plastic strains, and the high-cycle fatigue region, where macroscopic stresses and strains are still limited to the purely elastic behaviour of the material.

For high-cycle fatigue there are different calculation criteria based on the stresses, which relate the number of cycles to failure to a stress-based parameter representative of the stress level to which the material is subjected. With large plastic strains, as in the case of low-cycle fatigue, more complex criteria based on strains or strain energy must be used.

The widely used strain-based Manson-Coffin fatigue criterion relates the number of cycles to failure of a component to the applied plastic strain amplitude. This criterion is particularly suitable for situations where high loads induce high plastic strains in the material, thus leading to a low-cycle fatigue life. Isothermal fatigue tests controlled in strain are employed to define suitable parameters for the application of this criterion as a function of the operating temperature, which is kept constant throughout each test.

Although these tests are more complex in terms of test management and control compared for example to traditional rotary bending for high cycle fatigue tests, they constitute a routine in low cycle fatigue investigation. Nevertheless, considering the specific case of exhaust manifolds, a complication emerges linked to the actual conditions of use and the related operating temperature cycle. The cyclic stresses and strains in the component are mainly promoted by the temperature variation along the loading cycle and by the corresponding thermal gradients. Therefore, the fatigue parameters obtained on specimens subjected to a constant and uniform temperature are no longer accurate. It would be necessary to make simplifying assumptions such as defining an average or maximum cycle temperature as a reference parameter for fatigue life estimation [24]. Moreover, a further complication is introduced by the fact that exhaust manifolds present complex geometries and are usually subjected to multiaxial stress states. In this situation, energy-based criteria appear to be more suitable for thermal low-cycle fatigue calculations [17].

In this paper, the criterion based on the dissipated energy per cycle has been considered as the basis for justifying the use of a simplified criterion, which adopts the equivalent plastic strain range as a fatigue parameter and which has been then employed in the experimental/numerical correlations.

3.1.1. Dissipated energy criterion

From the pertinent literature [17,18,25–27], it is known that there is a relationship between the fatigue life of a material and the plastic hysteresis loop to which it is subjected [28]. The relationship between plastic work ΔW_p and fatigue life is of the type:

$$\Delta W_p = K' \bullet N_f^{\alpha'} \tag{1}$$

where N_f is the number of cycles to failure and K' and α' are characteristic parameters of the material and must be obtained experimentally through isothermal and non-isothermal characterizations controlled in strain.

As a basic theory, the area of the hysteresis loop is equal to the plastic strain work per unit volume produced during one load cycle, see Fig. 16. This work is partly dissipated through heat and partly stored in the material in the form of sliding on crystalline planes and dislocations which can cause possible damage and nucleation of fatigue cracks.

The total hysteresis energy can be defined as the sum of all hysteresis cycles in the life of a component. Neglecting the initial phase of possible hardening or softening of the material, the total energy can be considered equal to the product of the area of the stabilized hysteresis cycle by the number of cycles to failure.

The area of the hysteresis cycle, Fig. 16(b), is usually expressed as:

$$\Delta W_p = \int \sigma \bullet d\varepsilon_p \tag{2}$$

where ε_p is the plastic strain.

3.1.2. Equivalent plastic strain range (ΔPEEQ)

In the case of very low-cycle fatigue, an extremely simple criterion based on plastic strains only can be adopted and its validity can be related, albeit approximatively, to the more robust energetic approach briefly reviewed in the previous section. In fact, considering the energy criterion theory and assuming an elastic-perfectly plastic material behaviour, i.e. $\sigma_a \cong \sigma_y$, Eq. (2) becomes (see Fig. 16(b)):

$$\Delta W_p = \Delta\sigma\Delta\varepsilon_p = 2\sigma_a 2\varepsilon_{ap} = 4\sigma_y\varepsilon_{ap} \tag{3}$$

Since yield stress σ_y is a usually available common characteristic of the material as a function of the temperature, one could say that, for a given temperature, the plastic strain energy only depends on the plastic strain. In fact, the almost rectangular area of the hysteresis loop can be calculated by the product of the height, which is twice the yield stress, and the base, which is the plastic strain range, see Eq. (3).

The elastic-perfectly plastic material assumption used to justify the derivation of Eq. (3) is certainly a crude hypothesis, but in the case of stainless steels used at high temperatures (above 800 °C), it may not deviate too much from real stress/strain curves profiles, see Figs. 14 and 15.

Since this contribution aims at identifying a simple criterion to be correlated with the practical experience gained over the years with Ferrari engines, useful considerations can be derived from tests carried out on the exhaust manifolds. In particular, the operating temperature typically reached by manifolds at the critical locations during testing is confined in the range of 750–850 °C thus limiting the range of variation of the yield stress and corroborating the hypothesis that fatigue is governed only by plastic strains as suggested by Eq. (3).

Practically, the range of equivalent plastic strain (ΔPEEQ) for a single thermal cycle, easily derivable from FE analysis [29], is used to post-process the numerical results.

However, it is important to underline that this approach cannot be generalised. The defined trends strongly depend on the operating temperature and can only be considered valid if the conditions remain similar. In other words, it is certainly not a rigorous method, but it can be very effective in all those industrial situations with components that can have completely different geometries but are subject to similar conditions of use due to their function. This is the case of the exhaust manifolds mounted on the various applications of the Ferrari V8 engines.

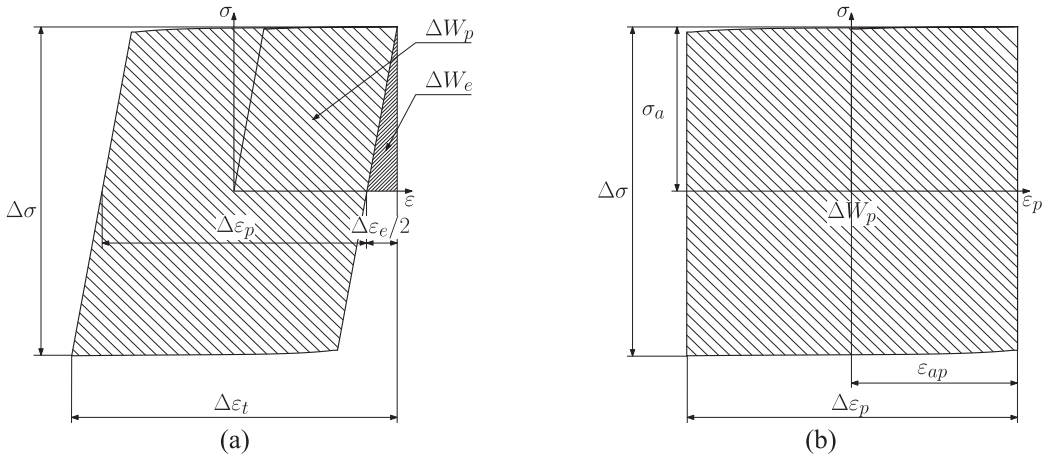

Fig. 16. Almost elastic-perfectly plastic material: a) elastoplastic hysteresis cycle, b) plastic hysteresis cycle.

4. Calculation

4.1. Finite Element analyses

The proposed modelling strategy has been divided into two main phases. First, a thermal analysis of the system has been performed to closely replicate the specific temperature cycling of the Thermal Shock and Engine Life tests. Then, a decoupled thermal - thermo-structural model has been prepared to estimate the stress state of the component as a function of the applied temperature history.

All numerical analyses have been performed using the commercial Finite Element software Abaqus.

The simulations include the components necessary for the correct determination of the temperatures, without neglecting any detail that could influence the stress state of the manifold. In fact, a node-to-node correspondence of the thermal and structural model has been employed to avoid interpolations of the temperature range, which are usually managed independently by the software. In particular, the engine head, the manifold and the turbine have been considered. Furthermore, the connection detail between the manifold and the head has been added by modelling studs, nuts, gasket and all the anti-unscrewing systems. The applications analysed do not have bracket or support systems as the turbocharger unit is supported directly by the manifold.

Two distinct V8 engine models named B and C engine with various geometric variations have been considered. The B1 and C1 versions refer to the initial development geometries which presented anomalies during the experimental tests, while B2 and C2 indicate the validated solutions which have been adopted in the final design. For all the configurations considered, the relative models of both engine banks (right and left) have been generated, but, for the sake of brevity, the results of only one bank will be presented in the following. Figs. 17 and 18 show the exhaust manifold mounted during the validation tests and the corresponding calculation model of the C1 and B1 engines respectively.

The examined exhaust manifolds have been produced by casting using the custom developed cast steel referred as Steel 2 in Section 2.3. All the main material properties have been considered temperature dependent in order to obtain reliable and meaningful numerical results (see Figs. 19 and 20). In particular, the mechanical properties, discussed in detail in Section 2.3, have been normalised here with respect to the ambient temperature condition, while physical properties have been retrieved from the data available in the literature [30] and from those supplied directly by the foundry that manufactured the component and also in this case they have been here normalised with respect to the ambient temperature condition.

The behaviour of the material has been simulated through a bilinear elasto-plastic model with kinematic hardening. Kinematic hardening has been chosen to simulate the behaviour of the material subjected to cyclic loading and it is fundamental for the study of thermal fatigue phenomena where plastic strains prevail. This hardening model considers the boundary surface of the yield stress moving into the stress space, so a deformation in one direction reduces the yield stress in the opposite direction. This simulates the Bauschinger effect [31] and the work-hardening induced anisotropy, which are necessary conditions for correctly capturing the hysteresis loops of the material with cyclic plastic strain. Specifically, linear kinematic hardening and yield stress boundary surface model described by von Mises equivalent stress have been used in the analysis.

Possible isotropic hardening or softening can also affect the shape and dimensions of the stress–strain hysteresis cycle and can consequently modify the amount of energy absorbed by the material for a given equivalent plastic strain range. Nevertheless, the authors decided to ignore this contribution in the simulations and to adopt material parameters derived by the monotonic tensile tests to feed the numerical models. A discussion can be made to support this decision. In fact, in this activity, the numerical simulations are directly correlated to failures registered in actual components with different geometries but manufactured with the same material. Consequently, if we compare two different geometries exhibiting similar plastic strain ranges and temperatures, possible hardening or softening of the material can have a comparable influence making the results to be still reliable at least in relative terms. Moreover, results can be found in the literature[32] where cyclic tests performed of materials with a chemical composition close to the one of the material considered in this application showed limited isotropic hardening or softening.

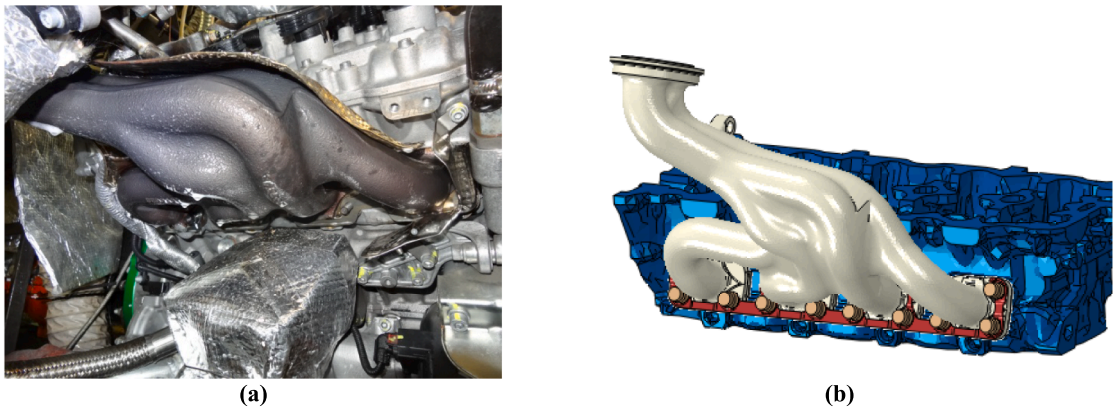

(a) (b)

Fig. 17. Engine C1 - (a) Detail of the right-hand side exhaust manifold; (b) Finite Element model.

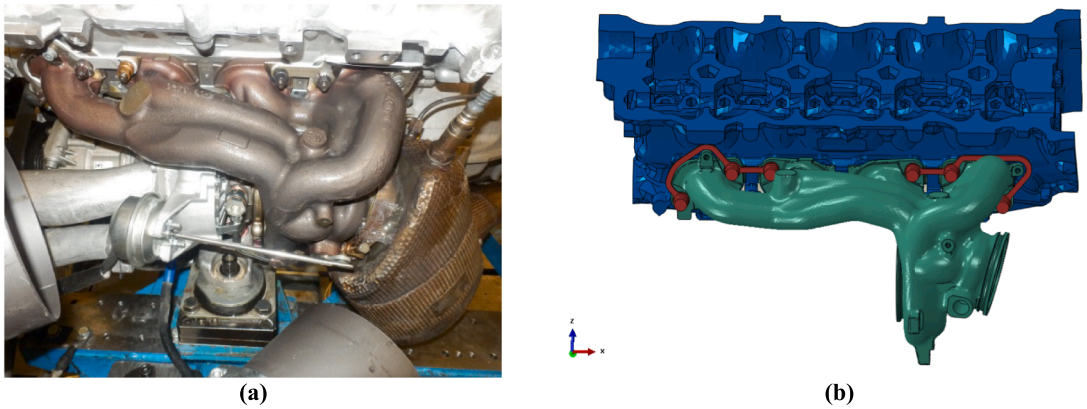

Fig. 18. Engine B1 - (a) Detail of the left-hand side exhaust manifold; (b) Finite Element model.

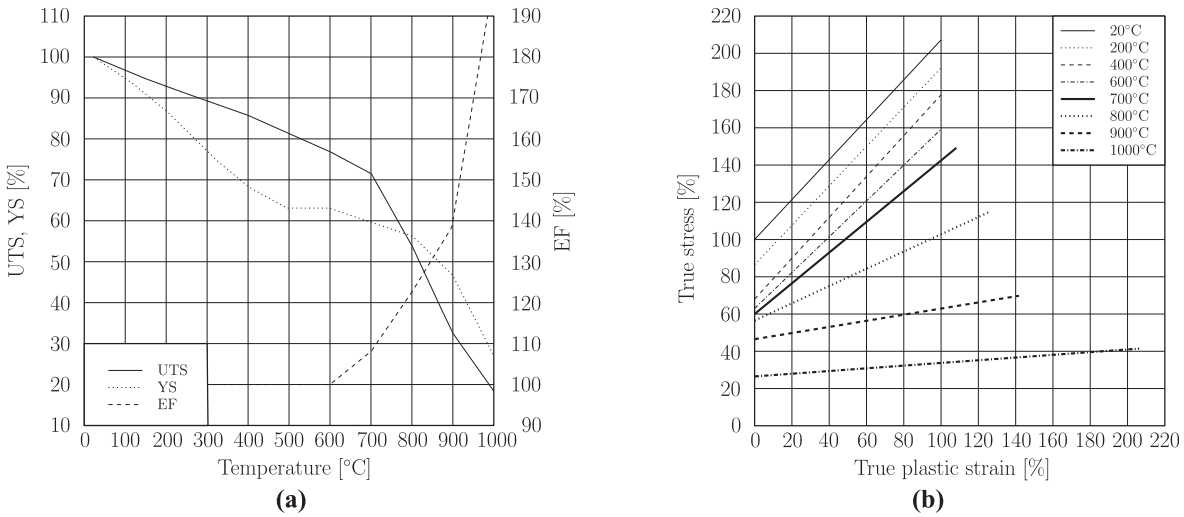

Fig. 19. (a) Mechanical properties as a function of temperature; (b) plastic region of the bilinear elastoplastic model adopted.

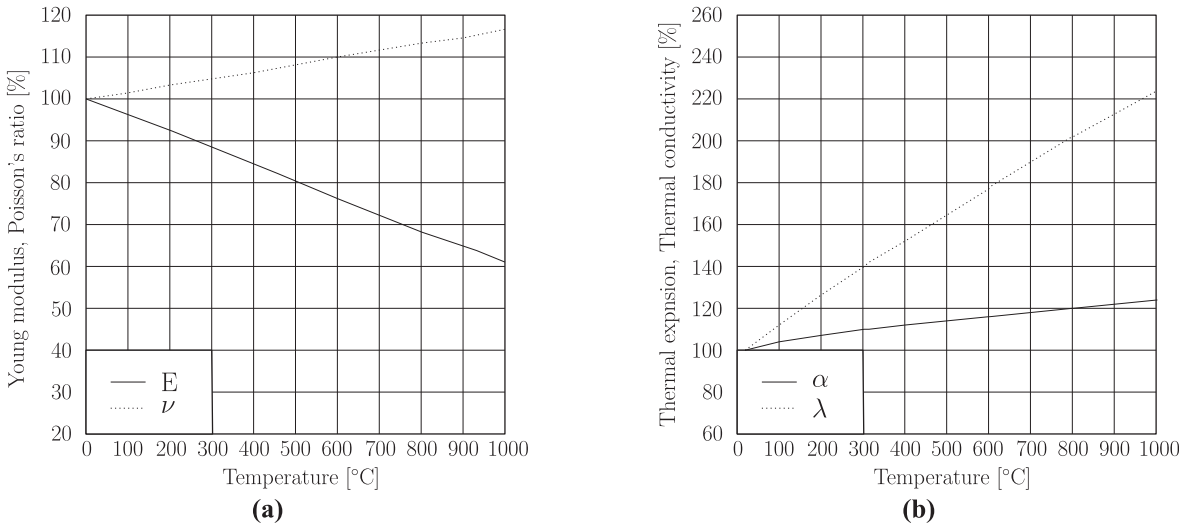

Fig. 20. (a) Mechanical properties as a function of temperature; (b) physical properties as a function of temperature.

5. Results

5.1. Thermal model

The simulations include a series of thermal transient analyses to replicate Ferrari *Engine Life* and *Thermal Shock* validation cycles. The thermal results have been subsequently used as input in the structural model for the evaluation of the stress state along the entire loading history.

The model used to obtain the manifold thermal field considered boundary conditions related to the exhaust gasses inside the manifold and to the external airflow surrounding the engine [33,34]. In particular, the convention exchanges both on the internal surface of the duct and on the external surfaces have been set to respectively mimic the contribution of the exhaust gases and of the forced cooling air. Simulation tools, such as 3D fluid dynamics analysis or 1D heat transfer analysis, have been used to define these boundary conditions, the details of which are beyond the scope of this contribution. Conduction has been then added between the parts in contact using suitable thermal resistances. As a last boundary condition, a constant temperature of 150 °C has been imposed on the head and a specific contact resistance has been defined at the interfaces with the gasket.

Fig. 21 identifies the different surfaces that define the areas of application of the boundary conditions for the thermal analysis of the manifold of engine C1.

In the thermal transient simulations, two distinct operating conditions have been considered between the heating and cooling phases, which are activated in succession to simulate the complete thermal cycle. To reach the steady-state thermal condition it has been necessary to simulate a sequence of at least five complete cycles, see Fig. 22. These analyses have been performed for each exhaust manifold configuration and for each different test condition.

The results of the thermal analyses have been then compared with the experimental evidence.

Figs. 23 and 24 show the maximum and minimum temperatures calculated for the C1 engine over the *Engine Life* cycle. A numerical/experimental comparison referring to the 18 measured points is presented. The temperature distribution is satisfactorily captured both in the heating and cooling phases of the cycle; the percentage difference is in the range of 2–3%.

To further validate the methodology, two more analyses of the C1 and B1 engines have been performed for the *Thermal Shock* cycle.

Figs. 25 and 26 compare the temperature trends calculated in the *Thermal Shock* cycle with the experimental measurements. It can be seen that the methodology has successfully replicated the test conditions.

5.2. Thermomechanical model

The thermomechanical model has been used to mimic the effect of the thermal cycles of the various Ferrari validation tests on the exhaust manifold in terms of stress and strain.

Thermomechanical analyses referred to quasi-static simulations require a succession of thermal states that represent the different time instants of heating and cooling phases of the complete cycle. Since the behaviour of the elastoplastic model of the material is highly nonlinear, the result depends not only on the initial and final state of the cycle but on the entire temperature history. It is evident that the discretization of the cycle is a fundamental parameter. Therefore, each heating and cooling phase has been discretized using at least eight increments.

Both the *Engine Life* and *Thermal Shock* thermal cycle have been repeated five times to obtain a stable behaviour, unaffected by the first heating phase.

Fig. 27 shows the PEEQ Equivalent Plastic Strain trends during the application of the five thermal cycles at three different locations of a generic manifold. Two main scenarios can be identified. Points A and B exhibit a plastic strain at the first heating and a constant increase in PEEQ for each subsequent cycle applied. Point C shows only an initial plastic strain which remains unchanged in subsequent cycles. Of greater interest is the first case, where the constant increase of PEEQ for each heating and cooling phase is a symptom of repeated plastic strains and is attributable to a hysteresis cycle of the material. The calculation model, therefore, is able to simulate the fundamental phenomenon that governs cyclic damage due to thermal fatigue.

In the following, comparisons between the ΔPEEQ results calculated for each case and the experimental evidence are presented. For company confidentiality policy, the results in terms of ΔPEEQ have been normalized with respect to the maximum value registered in the simulations to make them still directly comparable.

Fig. 28 compares the results of the *Engine Life* cycle for engine C1. The area around the central massive part (casting ingate mark) shows a cyclic plastic strain. In particular, the calculation shows the maximum ΔPEEQ points located on the internal surfaces of the ducts, in agreement with the fatigue trigger indicated by laboratory analysis (see Fig. 8).

Fig. 29 compares the results of the *Thermal Shock* cycle. The C1 engine showed anomalies after 400 cycles and the Finite Element model shows critical areas located in the same position.

Figs. 30 and 31 refer to the B1 engine which has been tested following only the *Thermal Shock* cycle. The rupture highlighted after 500 cycles is well represented by the numerical model.

The numerical approach developed has been then employed to guide a possible geometric optimization of the component. Several iterations have been performed and satisfactory final designs have been achieved for both engine configurations C and B, i.e. engine configurations C2 and B2. Figs. 32 and 33 show that the cyclic plastic strain range ΔPEEQ decreases significantly compared to the starting geometries B1 and C1. The geometric modifications introduced have been specifically defined to limit stresses during thermal transients. Extensive use has been made of the FE calculation methodology to identify the best compromise between the production, performance and reliability requirements of the component. For example, in relation to the manifold of the C2 engine, the authors have

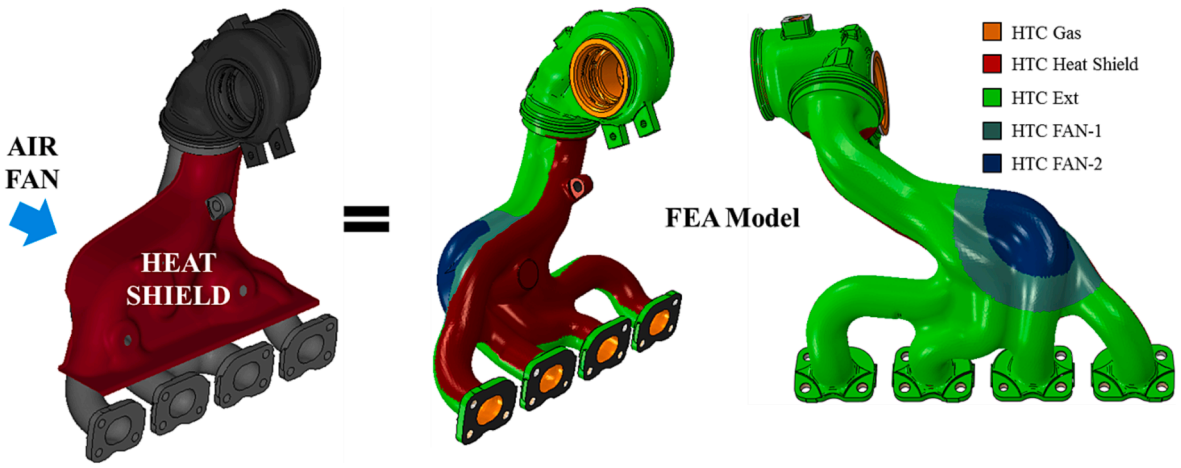

Fig. 21. Thermal boundary condition applied to the exhaust manifold of the C1 engine.

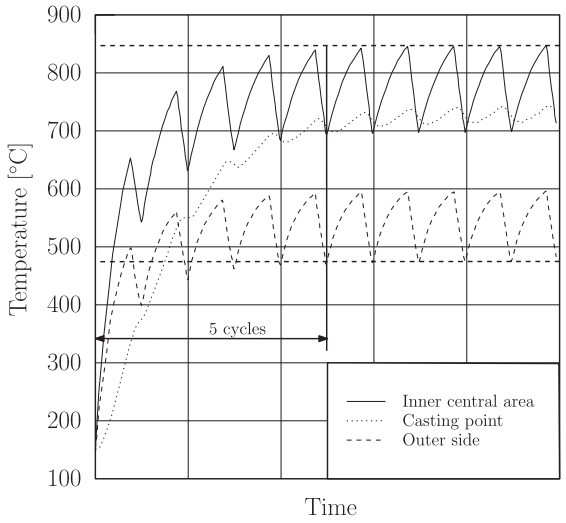

Fig. 22. Trend of simulated temperatures of the exhaust manifold of the C1 engine.

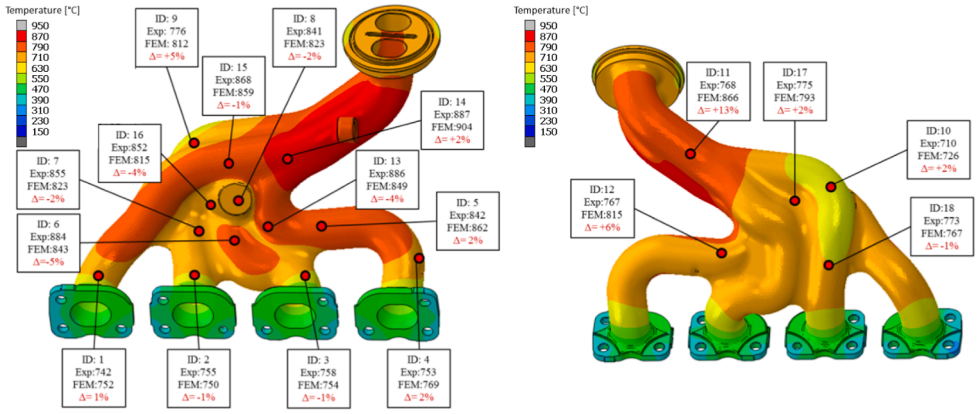

Fig. 23. Engine C1 - Experimental/Numerical comparison; *Engine Life* cycle, maximum temperatures.

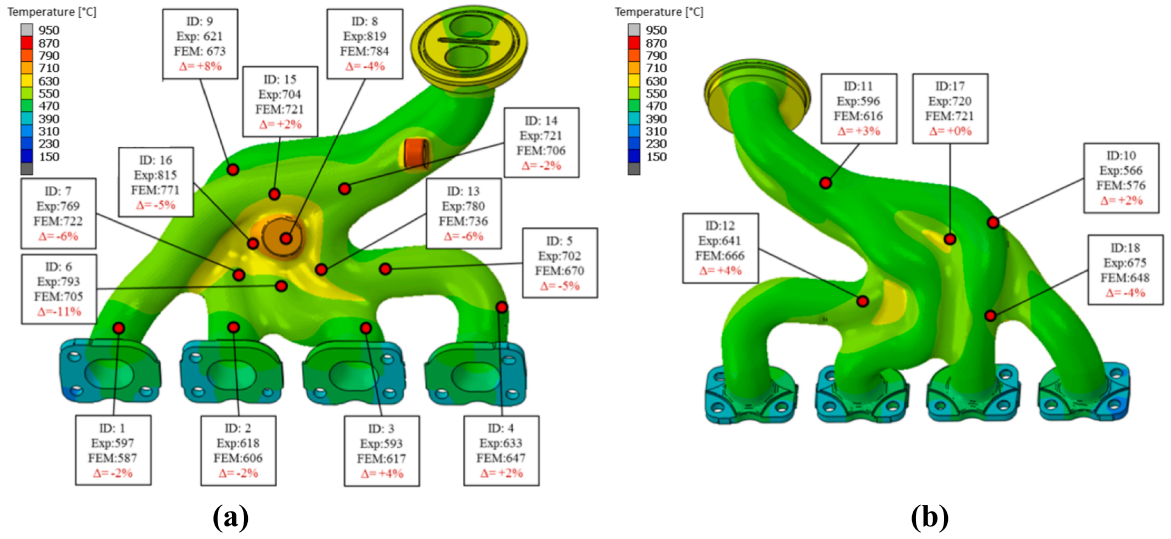

Fig. 24. Engine C1 - Experimental/Numerical comparison; *Engine Life* cycle, minimum temperatures.

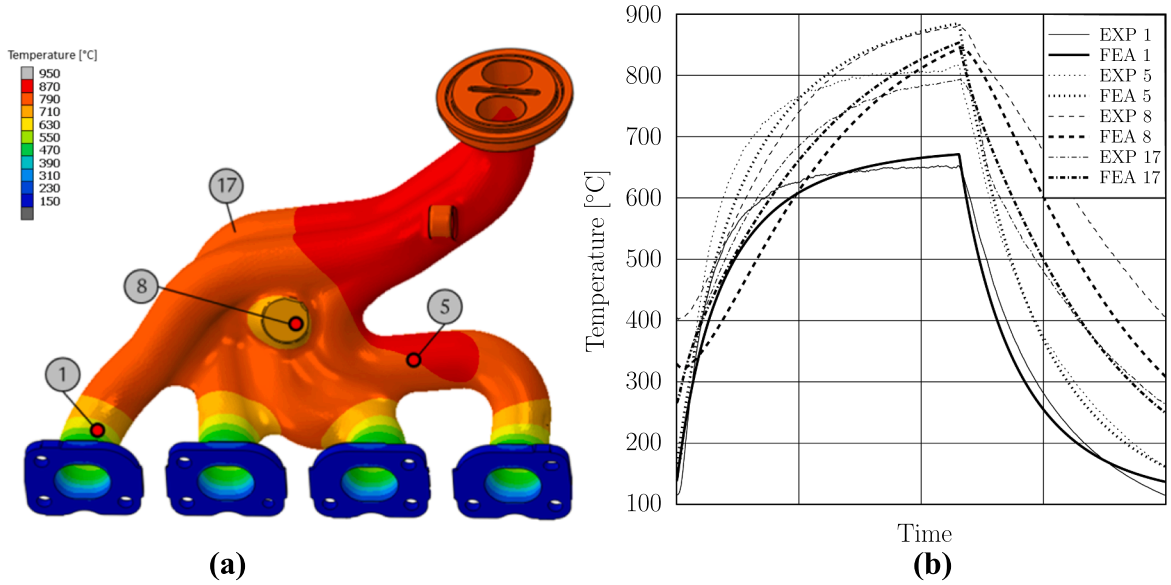

Fig. 25. C1 Engine - Experimental/Numerical comparison; *Thermal Shock* cycle.

tried to limit as much as possible the central mass, necessary for the correct feeding of the metal during the casting process, in order to obtain uniform temperature gradients and reduce thermal stresses, see point A of Fig. 32. Instead, in the B2 engine configuration, the section variation between the thin wall of the volute and the fixing stud housing has been made more gradual, see point A of Fig. 33. To prove the validity of the numerical models, the final geometries C2 and B2 have been also experimentally verified, and the tests have been successfully completed.

6. Discussion

Considering the results of the FE models and the engine bench tests in terms of number of cycles to failure, a specific fatigue chart has been derived which summarizes the experiences acquired by Ferrari during these validations. In particular, all the tests carried out on the two engines C and B have been examined, each in the two different geometrical variants, i.e. exhaust manifold at the beginning of the development process (C1 and B1) and experimentally validated final geometries (C2 and B2).

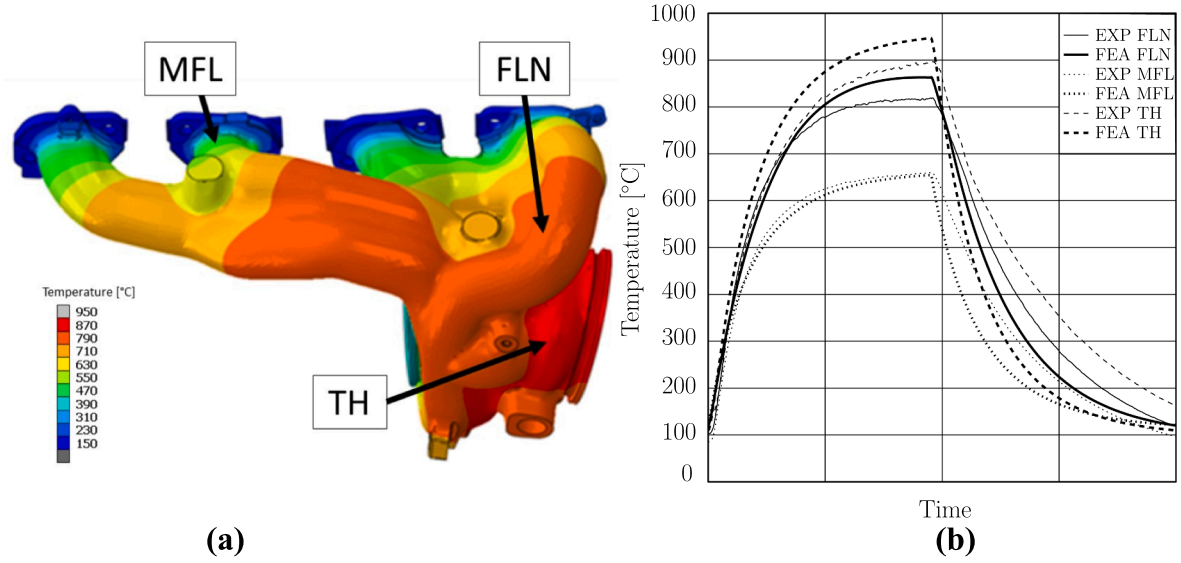

Fig. 26. B1 Engine - Experimental/Numerical comparison; *Thermal Shock* cycle.

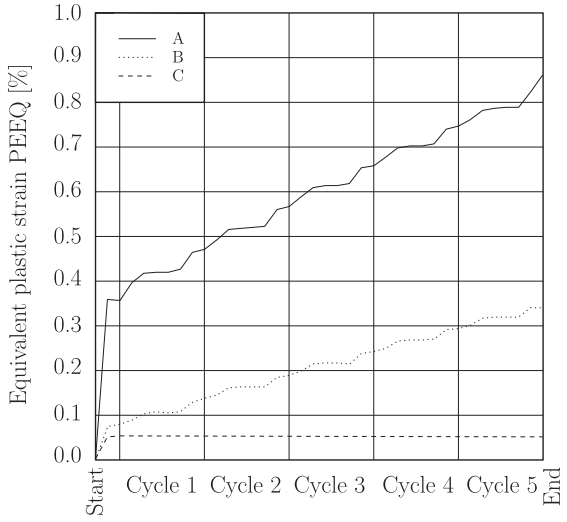

Fig. 27. Trend of the Equivalent Plastic Strain PEEQ during five thermal cycles at different locations.

6.1. C engine

In the C engine variants, both the *Thermal Shock* and *Engine Life* validation tests have been considered. In particular, similar ruptures were found in both test cycles. In fact, the less severe *Engine Life* cycle extended the life of the component by shifting thermal fatigue failures to a higher number of cycles.

Fig. 34 illustrates the fatigue diagram derived considering the experimental tests performed on engine variants C1 and C2. Specifically, the diagram has been derived as follows:

a) First, tests in which failures have been detected (C1 configuration) have been considered and, in the interest of safety, the minimum number of cycles to failure have been used to populate the diagram, i.e. 400 cycles for the *Thermal Shock* test and 6300 cycles for the *Engine Life* test, see Section 2.2.1;
b) Then, for all the points at which a fatigue crack has been observed, the corresponding equivalent plastic strain range has been extracted from the numerical simulations and, again in the interest of safety, only the values higher than 80% of the maximum registered in the simulation referring to the specific test have been used to populate the diagram, i.e. 2 points for the *Thermal Shock* test and 1 point for the *Engine Life* test, see black □-marks;

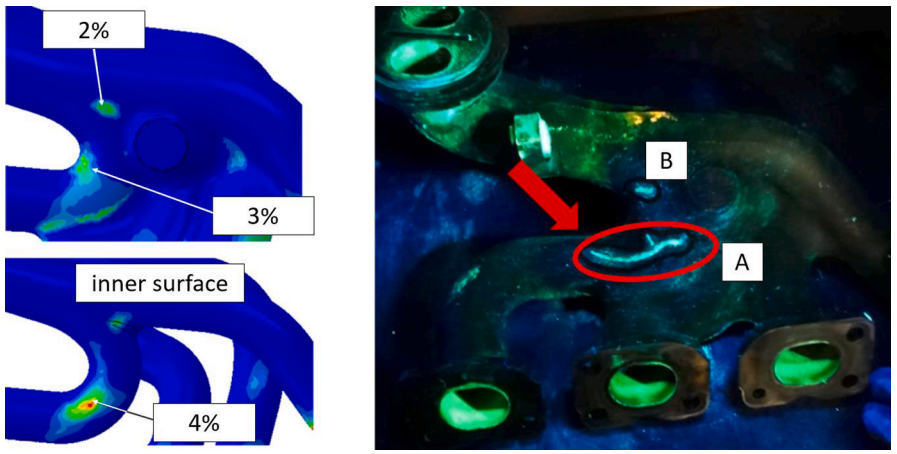

Fig. 28. ΔPEEQ calculated for engine C1 exhaust manifold in the *Engine Life* cycle. Comparison with cracks highlighted by dye penetrant tests after 150 h (6300 thermal cycles).

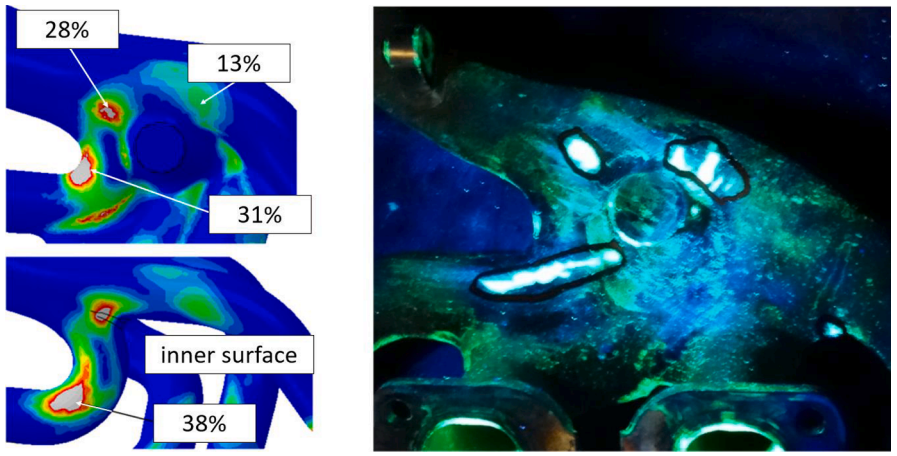

Fig. 29. ΔPEEQ calculated for engine C1 exhaust manifold in the *Thermal Shock* cycle. Comparison with cracks highlighted by dye penetrant tests after 400 cycles.

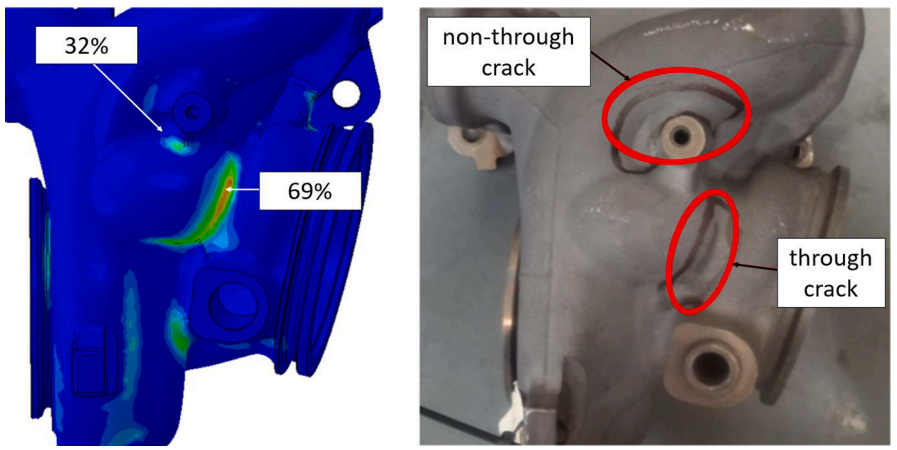

Fig. 30. ΔPEEQ calculated for engine B1 exhaust manifold in the *Thermal Shock* cycle.Comparison with cracks highlighted after 500 cycles.

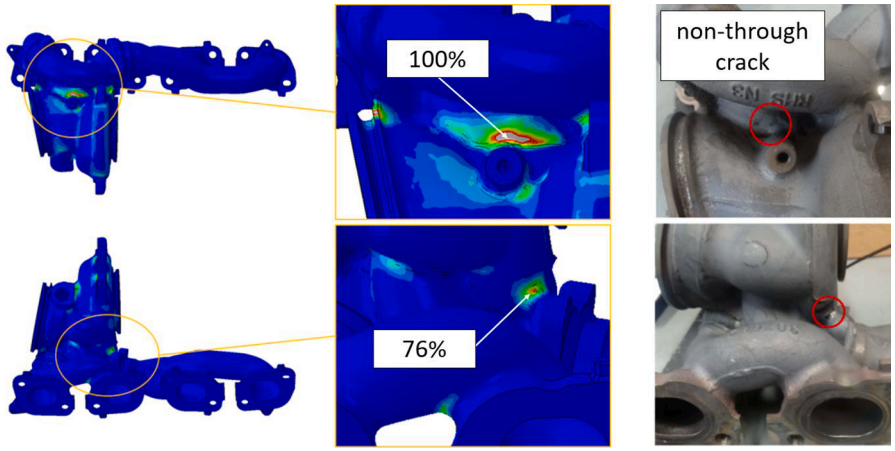

Fig. 31. ΔPEEQ calculated for engine B1 exhaust manifold in the *Thermal Shock* cycle.Areas with recurring fatigue failures at the end of the test.

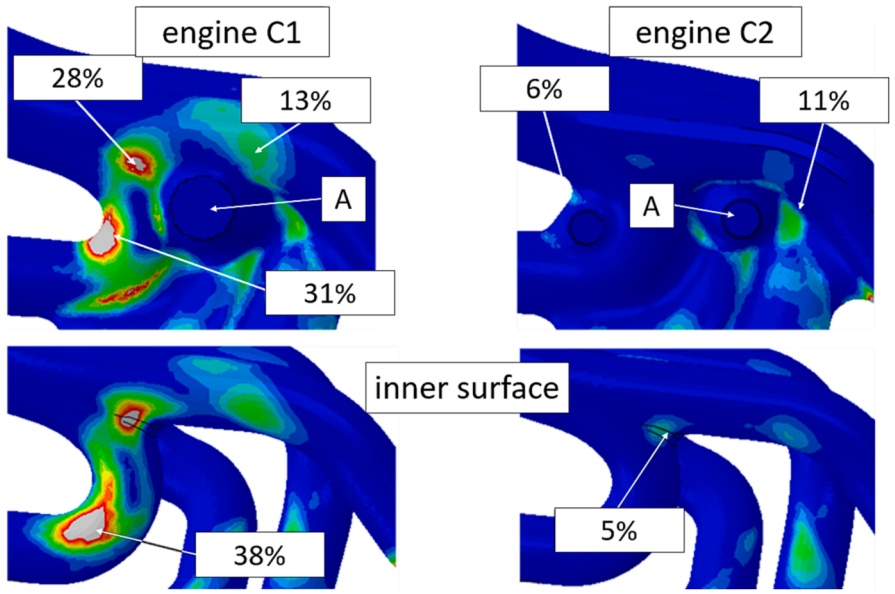

Fig. 32. ΔPEEQ calculated for the exhaust manifold of engine C2 in the *Thermal Shock* cycle.

c) Additionally, only for the *Thermal Shock* test, points at which a non-zero equivalent plastic strain range has been registered in the numerical simulation, but not exhibiting any failure during the inspection of the component when the test has been prematurely interrupted after 400 cycles, have been included in the diagram to have preliminary information about the amount of the tolerable equivalent plastic strain range for that specific number of cycles. In particular, the maximum value of the equivalent plastic strain range corresponding to a point at which no cracks have been observed has been derived by the simulation and only values higher than 80% of this limit have been used to populate the diagram, i.e. 3 points, see black ○-marks;
d) Finally, results of the equivalent plastic strain range at the same locations identified above have been reported in the diagram for the geometrically improved C2 variant which has successfully passed both tests without any crack, i.e. 5 points for the *Thermal Shock* test at 1000 cycles, two points are almost overlapping, and 1 point for the *Engine Life* test at 7500 cycles, see black x-marks.
e) Once all the points have been introduced in the diagram a linear trend has been identified linking the points corresponding to the failed locations, see the dotted line.

6.2. B engine

In the B engine variants, only the *Thermal Shock* validation tests have been considered.
Fig. 35 presents the experimental test results for the engine variant B1 and B2 and it has been derived as follows:

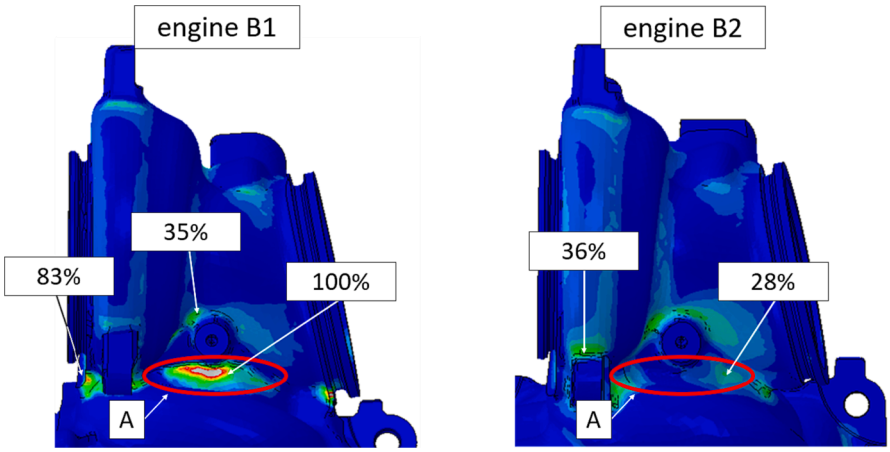

Fig. 33. ΔPEEQ calculated for the exhaust manifold of engine B2 in the *Thermal Shock* cycle.

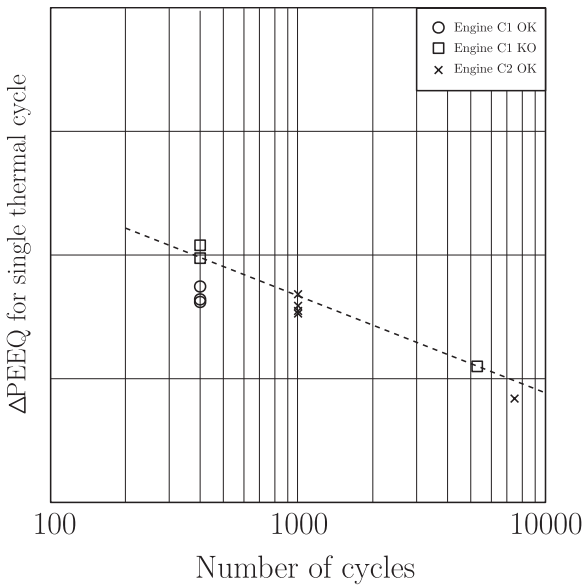

Fig. 34. ΔPEEQ and experimental cycles to failure of Engine C1 and C2.

a) First, tests in which failures have been detected (B1 configuration) have been considered and, in the interest of safety, the minimum number of cycles to failure have been used to populate the diagram, i.e. 500 cycles, see Section 2.2.2;
b) Then, for all the points at which a fatigue crack has been observed, the corresponding equivalent plastic strain range has been extracted from the numerical simulations and, again in the interest of safety, only the values higher than 80% of the maximum registered in the simulation referring to the specific test have been used to populate the diagram, i.e. 5 points, see black △-marks;
c) Finally, results of the equivalent plastic strain range at the same locations identified above have been reported in the diagram for the geometrically improved B2 variant which has successfully passed the *Thermal Shock* cycle without any crack, i.e. 5 points at 1000 cycles, see black + -marks. Two points are almost overlapping.
d) From the results corresponding to the engine variant B1 and B2 a clear trend cannot be identified since only *Thermal Shock* cycles have been performed. Nevertheless, the identified points have been superposed to the ones corresponding to engine variants C1 and C2 in order to verify a possible agreement, see Fig. 36.

6.3. Comparison

The complexity of managing a complete engine running on a bench excludes the possibility of constantly monitoring the structural integrity of the exhaust manifold during the test. For industrial test planning reasons, ruptures can only be detected through visual inspections at regular time intervals, see Section 2.2. In other words, there is always some variability and approximation in dating the

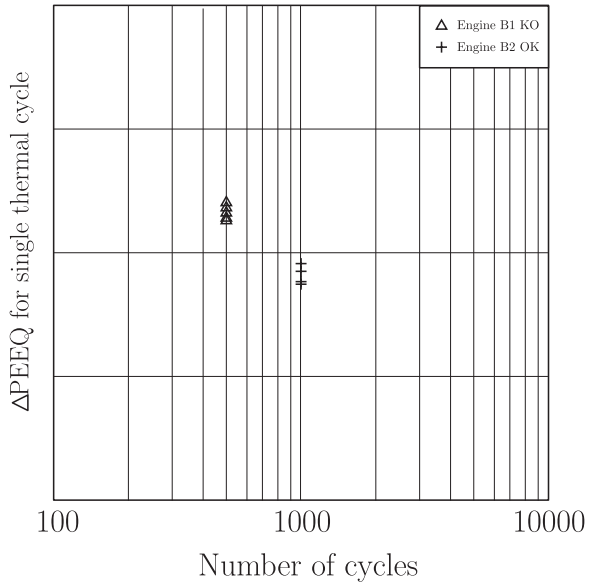

Fig. 35. ΔPEEQ and experimental cycles to failure of Engine B1 and B2.

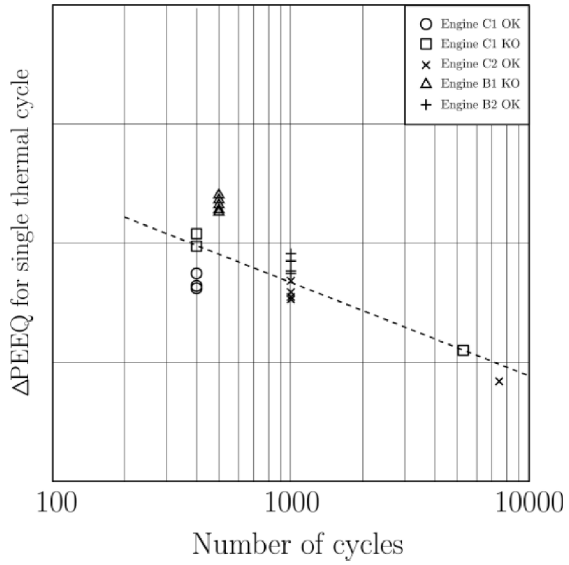

Fig. 36. Correlation between calculated ΔPEEQ and experimental cycles to failure for all engine configurations.

presence of fatigue cracks. Despite this discrete procedure, the results of Fig. 36 clearly identify a trend line between the ΔPEEQ parameter and the number of cycles to failure. Both configurations examined, B and C engines, show a similar trend, even if B engines seem to accept slightly higher ΔPEEQ values. This can be explained by considering the qualitative nature of the ΔPEEQ parameter and noting that the points where failures are detected in the two engines B and C have different maximum temperature values and therefore different values of yield stress (see Eq. (3)).

7. Conclusions and preventive actions

A methodology has been developed for the structural verification of exhaust manifolds for internal combustion engines with high specific power. In particular, thermal stresses and low-cycle fatigue phenomena have been addressed.

A dedicated experimental campaign has been performed to gain a deeper understanding of the mechanical properties of the material employed at different temperatures. In particular, a static characterization of the material has been carried out up to 1000 °C with the dual purpose of identifying an alloy with adequate mechanical characteristics and of having a necessary database to be used in

the subsequent Finite Element models. A cast stainless steel with a specific addition of niobium was selected to manufacture the exhaust manifold.

A suitable Finite Element numerical simulation strategy has been defined to mimic the experimental tests of the exhaust manifolds currently used by Ferrari. A virtual validation methodology has been defined to intercept and prevent possible structural problems before the physical realization of the components.

In the first simulation phase, a thermal model has been defined in the time domain which faithfully reproduces the temperature profile of the two specific Ferrari tests: *Engine Life* test and *Thermal Shock* test. Through dedicated experimental temperature measurements, it has been possible to calibrate and validate the model on two different manifold configurations, i.e. C and B engines.

In the second simulation phase, a decoupled thermal - thermo-structural model has been set up to estimate the stress state of the component as a function of the history of applied temperature. The purpose of the calculation models was to obtain a faithful representation of stresses and strains, both elastic and plastic, capable of describing the load history to which the component is subject during the validation tests. ΔPEEQ has been defined as the equivalent plastic strain range at a specific location of the component in a single thermal cycle under stable conditions. The results showed that ΔPEEQ is a parameter well correlated to recurring anomalies found in the early development geometries of the exhaust manifolds of the examined engines C1 and B1.

The developed simulation strategy has been then used to define the final manifolds geometries of C2 and B2 engines to minimize the ΔPEEQ parameter and it has been proved to be an effective method to guide the design of these components.

The cyclic plastic strain ΔPEEQ is assumed as a parameter of low-cycle fatigue damage, as it is proportional to the hysteresis loops that the material undergoes during the application of repeated heating and cooling cycles. The criterion is easy to be applied because the model requires only the static characteristics of the materials as a function of the temperature. There are no real theoretical goals to achieve, and the criterion needs to be fine-tuned against experimental evidence of thermal fatigue failure.

The results of Finite Element simulations and engine bench tests in terms of the number of cycles to failure have been finally employed to define a specific fatigue diagram which summarizes the experiences gained by Ferrari during these validations. A clear trend line has been identified between ΔPEEQ and the number of cycles to failure. The fatigue diagram and the results of the FE models define a tool capable of estimating the life of the exhaust manifolds in terms of the number of allowable cycles.

The fatigue criterion based on plastic strains should not be considered a generic criterion, but remains linked to the specific application examined. The defined trends strongly depend on the operating temperature and can only be considered valid if the conditions remain similar. The proposed method is certainly not rigorous, but it can be very effective in all those complex industrial situations where individual components (even with very different geometries) are subject to similar conditions of use due to the functional requirements of the assembly. This is precisely the case of the exhaust manifolds mounted on the various applications of the Ferrari V8 engines.

Declaration of Competing Interest

The authors declare that they have no known competing financial interests or personal relationships that could have appeared to influence the work reported in this paper.

Data availability

The authors do not have permission to share data.

References

[1] S. Sissa, M. Giacopini, R. Rosi, Low-cycle thermal fatigue and high-cycle vibration fatigue life estimation of a diesel engine exhaust manifold, Procedia Eng. 74 (2014) 105–112, https://doi.org/10.1016/j.proeng.2014.06.233.
[2] S. Fontanesi, M. Giacopini, Multiphase CFD-CHT optimization of the cooling jacket and FEM analysis of the engine head of a V6 diesel engine, Appl. Therm. Eng. 52 (2013) 293–303, https://doi.org/10.1016/j.applthermaleng.2012.12.005.
[3] M. Lorenzini, M. Giacopini, S.G. Barbieri, Thermo-Mechanical Analysis of the Exhaust Manifold of a High Performance Turbocharged Engine, Key Eng. Mater. 774 (2018) 307–312, https://doi.org/10.4028/www.scientific.net/KEM.774.307.
[4] L.G. Tan, G.L. Li, C. Tao, P.F. Feng, Study on fatigue life prediction of thermal barrier coatings for high-power engine pistons, Eng. Fail. Anal. 138 (2022), 106335, https://doi.org/10.1016/j.engfailanal.2022.106335.
[5] B. Salehnasab, J. Marzbanrad, E. Poursaeidi, Transient thermal fatigue crack propagation prediction in a gas turbine component, Eng. Fail. Anal. 130 (2021), 105781, https://doi.org/10.1016/j.engfailanal.2021.105781.
[6] E. Kamouri Yousefabad, S. Asadi, P. Savadkouhi, O. Sedaghat, A. Bakhshi, The effect of non-uniform combustion temperature profile on thermal fatigue cracking of an air-cooled gas turbine vane, Eng. Fail. Anal. 105 (2019) 766–780. https://doi.org/10.1016/j.engfailanal.2019.07.008.
[7] V. Mangeruga, M. Giacopini, S.G. Barbieri, F. Berni, E. Mattarelli, C. Rinaldini, Design of a Hybrid Power Unit for Formula SAE Application: Packaging Optimization and Thermomechanical Design of the Electric Motor Case, SAE Technical Paper Series (2019), https://doi.org/10.4271/2019-24-0197.
[8] S.G. Barbieri, M. Giacopini, V. Mangeruga, S. Mantovani, Design of an Additive Manufactured Steel Piston for a High Performance Engine: Developing of a Numerical Methodology Based on Topology Optimization Techniques, SAE Int. J. Engines 11 (2018), https://doi.org/10.4271/2018-01-1385.
[9] H. Katori, M. Arai, K. Ito, Comprehensive Numerical Simulation of Stress and Damage Fields under Thermo-Mechanical Loading for TBC-Coated Ni-Based Superalloy, Key Eng. Mater. 774 (2018) 137–142, https://doi.org/10.4028/www.scientific.net/KEM.774.137.
[10] A. Benoit, M.H. Maitournam, L. Rémy, F. Oger, Cyclic behaviour of structures under thermomechanical loadings: Application to exhaust manifolds, Int. J. Fatigue 38 (2012) 65–74, https://doi.org/10.1016/j.ijfatigue.2011.11.012.
[11] E. Charkaluk, A. Bignonnet, A. Constantinescu, K. Dang Van, Fatigue design of structures under thermomechanical loadings, Fatigue Fract. Eng. Mater. Struct. 26 (2003) 661, https://doi.org/10.1046/j.1460-2695.2002.00613.x-i1.
[12] X. Luo, P. Zou, X. Zeng, X. Yuan, B. Li, H. Teng, Y. Xu, Failure Prediction and Design Optimization of Exhaust Manifold based on CFD and FEM Analysis, SAE Technical Papers. 2020-April (2020) 1–8. https://doi.org/10.4271/2020-01-1166.

[13] Ms.N.N. Shinde, Thermal Fatigue Analysis of Exhaust Manifold, Int. J. Res. Appl. Sci. Eng. Technol., 8 (2020) 370–378. https://doi.org/10.22214/ijraset.2020.32137.
[14] S.G. Barbieri, V. Mangeruga, M. Giacopini, M.S. Callegari, L. Bagnoli, Effect of the Thermal Mean Stress Value on the Vibration Fatigue Assessment of the Exhaust System of a Motorcycle Engine, SAE Int. J. Engines 16 (2023), https://doi.org/10.4271/03-16-08-0057.
[15] Z. Yan, L. Zhien, X. Wang, H. Zheng, Y. Xu, Cracking Failure Analysis and Optimization on Exhaust Manifold of Engine with CFD-FEA Coupling, SAE Int. J. Passenger Cars Mech. Syst. 7 (2014) 873–881, https://doi.org/10.4271/2014-01-1710.
[16] M. Chen, Y. Wang, W. Wu, J. Xin, Design of the Exhaust Manifold of a Turbo Charged Gasoline Engine Based on a Transient Thermal Mechanical Analysis Approach, SAE Int. J. Engines 8 (2014), https://doi.org/10.4271/2014-01-2882.
[17] E. Charkaluk, A. Constantinescu, Energetic approach in thermomechanical fatigue for silicon molybdenum cast iron, Mater. High Temp. 17 (2000) 373–380, https://doi.org/10.1179/mht.2000.17.3.001.
[18] A. Constantinescu, E. Charkaluk, G. Lederer, L. Verger, A computational approach to thermomechanical fatigue, Int. J. Fatigue 26 (2004) 805–818, https://doi.org/10.1016/j.ijfatigue.2004.01.006.
[19] S.S. Manson, G.R. Halford, Fatigue and Durability of Metals at High Temperatures, ASM, International (2009), https://doi.org/10.31399/asm.tb.fdmht.9781627083430.
[20] L. Moro, D. Benasciutti, F. De Bona, Simplified numerical approach for the thermo-mechanical analysis of steelmaking components under cyclic loading: an anode for electric arc furnace, Ironmaking & Steelmaking. 46 (2019) 56–65, https://doi.org/10.1080/03019233.2017.1339482.
[21] N. Fujita, K. Ohmura, M. Kikuchi, T. Suzuki, S. Funaki, I. Hiroshige, Effect of Nb on high-temperature properties for ferritic stainless steel, Scr. Mater. 35 (1996) 705–710, https://doi.org/10.1016/1359-6462(96)00214-X.
[22] P.-O. Santacreu, O. Cleizergues, C. Simon, P. Duroux, Design of stainless steel automotive exhaust manifolds, Revue de Métallurgie. 101 (2004) 615–620, https://doi.org/10.1051/metal:2004130.
[23] N. Fujita, K. Ohmura, A. Yamamoto, Changes of microstructures and high temperature properties during high temperature service of Niobium added ferritic stainless steels, Mater. Sci. Eng. A 351 (2003) 272–281, https://doi.org/10.1016/S0921-5093(02)00831-6.
[24] X. Su, M. Zubeck, J. Lasecki, C.C. Engler-Pinto, C. Tang, H. Sehitoglu, J. Allison, Thermal Fatigue Analysis of Cast Aluminum Cylinder Heads, in, SAE Technical Papers (2002) 418–424, https://doi.org/10.4271/2002-01-0657.
[25] V. Maurel, L. Rémy, F. Dahmen, N. Haddar, An engineering model for low cycle fatigue life based on a partition of energy and micro-crack growth, Int. J. Fatigue 31 (2009) 952–961, https://doi.org/10.1016/j.ijfatigue.2008.09.004.
[26] J.A. Abdalla, R.A. Hawileh, F. Oudah, K. Abdelrahman, Energy-based prediction of low-cycle fatigue life of BS 460B and BS B500B steel bars, Mater. Des. 30 (2009) 4405–4413, https://doi.org/10.1016/j.matdes.2009.04.003.
[27] S.-W. Kim, H.-S. Choi, B.-G. Jeon, D.-G. Hahm, Low-cycle fatigue behaviors of the elbow in a nuclear power plant piping system using the moment and deformation angle, Eng. Fail. Anal. 96 (2019) 348–361, https://doi.org/10.1016/j.engfailanal.2018.10.021.
[28] R.P. Skelton, Energy criterion for high temperature low cycle fatigue failure, Mater. Sci. Technol. 7 (1991) 427–440, https://doi.org/10.1179/mst.1991.7.5.427.
[29] ABAQUS, Abaqus 6.14, 2014.
[30] L. Vergani, Meccanica dei materiali (2006).
[31] M.-G. Lee, F. Barlat, Modeling of Plastic Yielding, Anisotropic Flow, and the Bauschinger Effect, in: Comprehensive Materials Processing, Elsevier, 2014, pp. 235–260, https://doi.org/10.1016/B978-0-08-096532-1.00219-3.
[32] M. Vinícius Pereira de Araújo, M. Corrêa de Carvalho, C. Olívio Figueiredo Terra Ruchert, Study of monotonic and cyclic mechanical behavior and microstructural evolution at a high temperature of ASTM A297 HP steel modified with niobium, Eng. Fail. Anal., 125 (2021) 105393. https://doi.org/10.1016/j.engfailanal.2021.105393.
[33] D.L. Li, Y.F. Yin, G.F. Chen, C. Cui, B. Han, Thermal Fatigue Analysis of the Engine Exhaust Manifold, Adv. Mat. Res. 482–484 (2012) 214–219, https://doi.org/10.4028/www.scientific.net/AMR.482-484.214.
[34] C. Liu, W.Z. Zhang, Lifetime Prediction of Thermo-Mechanical Fatigue for Exhaust Manifold, Adv. Mat. Res. 433–440 (2012) 9–17, https://doi.org/10.4028/www.scientific.net/AMR.433-440.9.